Biochemical and Biophysical Research Communications 413 (2011) 53–57

Contents lists available at SciVerse ScienceDirect

Biochemical and Biophysical Research Communications

journal homepage: www.elsevier.com/locate/ybbrc

Fluorescent metal nanoshell and CK19 detection on single cell image

Jian Zhang [a,*], Yi Fu [a], Ge Li [b], Joseph R. Lakowicz [a], Richard Y. Zhao [b,c,d,*]

[a] Center for Fluorescence Spectroscopy, University of Maryland School of Medicine, Department of Biochemistry and Molecular Biology, 725 West Lombard Street, Baltimore, MD 21201, USA
[b] Division of Molecular Pathology, Department of Pathology, University of Maryland School of Medicine, 10 South Pine Street, Baltimore, MD 21201, USA
[c] Department of Microbiology-Immunology, University of Maryland School of Medicine, 10 South Pine Street, Baltimore, MD 21201, USA
[d] Institute of Human Virology, University of Maryland School of Medicine, 10 South Pine Street, Baltimore, MD 21201, USA

ARTICLE INFO

Article history:
Received 3 August 2011
Available online 17 August 2011

Keywords:
Metal nanoshell
Plasmon resonance
Near-field interaction
Imaging agent
Fluorescent cell imaging
Time-resolved confocal microscope
Cytokeratin 19 (CK19)
Single molecule detection

ABSTRACT

In this article, we report the synthesis strategy and optical properties of a novel type of fluorescence metal nanoshell when it was used as imaging agent for fluorescence cell imaging. The metal nanoshells were made with 40 nm silica cores and 10 nm silver shells. Unlike typical fluorescence metal nanoshells which contain the organic dyes in the cores, novel metal nanoshells were composed of Cy5-labelled monoclonal anti-CK19 antibodies (mAbs) on the external surfaces of shells. Optical measurements to the single nanoparticles showed that in comparison with the metal free labelled mAbs, the mAb-Ag complexes displayed significantly enhanced emission intensity and dramatically shortened lifetime due to near-field interactions of fluorophores with metal. These metal nanoshells were found to be able to immunoreact with target cytokeratin 19 (CK19) molecules on the surfaces of LNCAP and HeLa cells. Fluorescence cell images were recorded on a time-resolved confocal microscope. The emissions from the metal nanoprobes could be clearly isolated from the cellular autofluorescence backgrounds on the cell images as either individuals or small clusters due to their stronger emission intensities and shorter lifetimes. These emission signals could also be precisely counted on single cell images. The count number may provide an approach for quantifying the target molecules in the cells.

1. Introduction

With advances in nanoscience and nanotechnology, noble metal nanoparticles are considered to be used as platforms for developing next generation nanoparticles with multiple functions [1,2]. Recently, there is an increasing interest in developing metal nanoparticles with magnetic and fluorescence properties for both magnetic resonance imaging (MRI) and fluorescence imaging [3–6]. In general, this kind of nanoparticle imaging probe is generated to contain γ-iron oxide nanoparticles in the cores for magnetic properties and also contain organic dyes for fluorescence properties. To increase the chemical stability and enrich the surface chemistry, the nanoparticles are often protected with silica or/and noble metal shells [7,8]. However, we also notice from the publications that in most cases, the organic dyes are simply incorporated with the iron oxide nanoparticles in the core [6–8]. As a result, the emission from the dyes is strongly quenched by the iron oxide components. In addition, it is uncertain whether there is any interaction between the dyes and iron oxide components in the cores that may reduce the constant magnetic properties of nanoparticles. Thus, there is an essential need to develop a new model of nanoparticles in which the organic dyes are immobilized separating from the iron oxide components and the magnetic and fluorescence properties of nanoparticles remain constant or even improved.

A near-field interaction of a fluorophore with a metal nanoparticle is known to be able to significantly improve optical properties of fluorophore [9–12]. Based on this observation, the metal nanoparticle probes are being developed for fluorescence cell imaging [13–15]. These metal nanoprobes are known to have increased emission intensity and decreased lifetime, as well increased photobleaching time and reduced photoblinking [16,17]. Typically, the metal nanoparticle probes are designed in two configurations: immobilizing the fluorophores on the external layers of metal spheres [18] or within the interior cores of metal nanoshells [19]. Since the iron oxide nanoparticles are needed to contain in the nanoparticle probes, the metal nanoshells rather nanospheres are used for designating new metal nanoparticle probes. We aim to reduce the organic dye-iron oxide interactions, so the organic dyes are consider to immobilize on the external layers of metal shells in this research (Fig. S1). According to the results of theoretical calculations [20,21], we understand that in addition a homogeneous electric field distribution in the core, there is an intensive distribution of electric field near the external area of metal nanoshell that

* Corresponding authors. Fax: +410 706 8409 (J. Zhang).
E-mail addresses: jian@cfs.biomet.umaryland.edu (J. Zhang), rzhao@som.umaryland.edu (R.Y. Zhao).

0006-291X/$ - see front matter © 2011 Elsevier Inc. All rights reserved.
doi:10.1016/j.bbrc.2011.08.042

can couple with the local organic dyes efficiently and result in greatly improved optical properties. The viewpoint was proved in the current research.

Novel metal nanoparticle probes were also conjugated with cytokeratin 19 (CK19) on LNCAP and HeLa cells for fluorescence cell imaging. Cytokeratins are a group of proteins in the intermediate filaments of epithelial cells [22]. According to recent reports, CK19 is known to express widely in various epithelia and release extensively by tumour cells [23,24], and thus, it is used as biomarker in epithelial malignancies. In addition, it is also a biomarker in lung carcinomas [25]. In this report, we determine the expression and distribution of CK19 in LNCAP and HeLa cells. Monoclonal anti-CK19 molecules (mAbs) were fluorescently labelled with Cy5 and the labelled mAb molecules were covalently bound on the external layers of silver nanoshells (Fig. S1). The formed mAb-Ag complexes were immuno-conjugated with the target CK19 molecules on the cell surfaces. The cell images were recorded on a time-resolved confocal microscope. The expression and distribution of CK19 on the cells were studied on the single cell intensity and lifetime images.

2. Materials and methods

All reagents and spectroscopic grade solvents were from Sigma-Aldrich and used as received. LNCAP and HeLa cells were obtained from the American Type Culture Collection (Manassas, Va.). Anti-CK19 mAbs were commercially available from Sigma-Aldrich. Cy5 mono NHS ester was purchased from Fischer Sci. Nanopure water (>18.0 MΩcm^{-1}) was purified with Millipore Milli-Q gradient system. (2-mercapto-propionylamino) acetic acid 2,5-dioxo-pyrrolidin-1-ylester was synthesized in a previous strategy [26].

2.1. Metal nanoparticle preparation and fluorescence labeling

Anti-CK19 mAbs were fluorescently labelled with Cy5 mono NHS ester via reactive ester reaction [27]. According to absorbance spectra, it was estimated that there was an average of 5.2 Cy5 molecules on each antibody molecule. Silica spheres with 40 nm diameters were synthesized in a modified Stöber strategy [28]. The surfaces of silica spheres were aminated by 3-aminopropyltrimethoxy silane and then deposited 10 nm thick silver nanoshells [29]. The silver nanoshells were recovered by centrifugation. They were subsequently coated with the organic monolayers of hexa(ethyleneglycol)mono-11-(acetylthio)undecyl ether to improve chemical stability and reduce non-specific interaction on cells during incubation [13]. To bind with the labelled antibodies, the silver nanoshells were partially substituted with (2-mercapto-propionylamino) acetic acid 2,5-dioxo-pyrrolidin-1-ylester *via* ligand exchange reaction [31]. Cy5-labelled antibodies were covalently bound on succinimidylated nanoparticles by co-dissolving mAbs in 10 mM phosphate buffered saline (PBS) buffer solution at pH 8.0 [32]. The formed mAb-Ag complexes were recovered by centrifugation and washed with 10 mM PBS buffer at pH 7.4.

2.2. Cell culture and conjugation

HeLa cells were maintained in Dulbecco's modified Eagle's medium (DMEM) supplemented with 10% fetal bovine serum (FBS). LNCaP cells were maintained in RPMI 1640 medium supplemented with 10% fetal bovine serum (FBS). The cell lines were immobilized on glass coverslips and washed with 10 mM PBS buffer at pH 7.4. The cell samples were then incubated with 1 nM mAb-Ag complexes, respectively, for 2 h in incubator. The nanoprobe-conjugated cells were washed with 10 mM PBS-Mg solution and dried in air for fluorescence cell imaging.

2.3. Spectral, imaging, and TEM measurements

Absorption spectra were collected on a Hewlett Packard 8453 spectrophotometer. Ensemble fluorescence spectra were performed on a Cary Eclipse Fluorescence Spectrophotometer. The imaging measurements were carried out on a time-resolved confocal microscope (MicroTime 200, PicoQuant). The measurement system consists of an inverted confocal microscope coupled to a

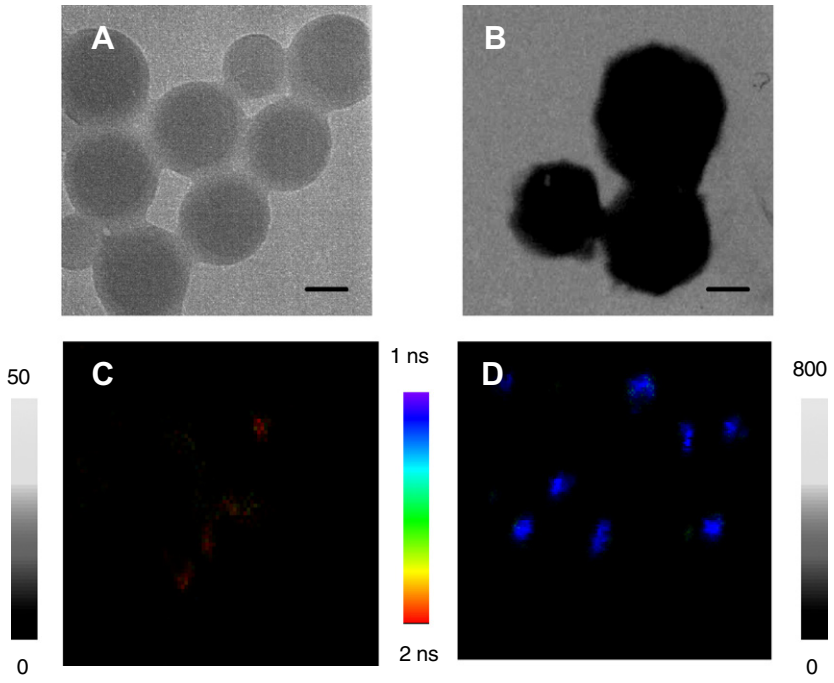

Fig. 1. Respective TEM images of (A) silica spheres and (B) metal nanoshells with scale bars of 20 nm, and typical emission intensity and lifetime images of (C) single metal free Cy5-labelled mAb molecules and (D) single metal nanoshells. The scales of C and D diagrams were 5 × 5 μm and the resolutions were 100 × 100 pixel with an integration of 0.6 ms/pixel.

high-sensitivity detection setup. A single mode pulsed laser diode (635 nm, 100 ps, 40 MHz) (PDL800, PicoQuant) was used as excitation light. An oil immersion objective (Olympus, 100×, 1.3NA) was used for both focusing laser light onto the sample and collecting fluorescence emission from the sample. The emission signal that passed a dichroic mirror was focused onto a 75 μm pinhole for spatial filtering to reject out-of-focus signal and recorded on a single photon avalanche diode (SPAD) (SPCM-AQR-14, Perkin Elmer Inc.). Bandpass filters were used to eliminate the excitation residue and to minimize spectral crosstalk. The data collected with a TimeHarp 200 board were stored in Time-Tagged Time-Resolved Mode (TTTR), which allows the detection of every photon with individual timing and channel information.

Transmission electron micrographs (TEM) were taken with a side-entry Philips electron microscope at 120 keV. Samples were cast from water solutions onto standard carbon-coated (200–300 Å) Formvar films on copper grids (200 mesh) by placing a droplet of a 1 mg/mL aqueous sample solution on grids. The size distribution of metal core was analyzed with Scion Image Beta Release 2 counting at least 200 particles.

3. Results and discussion

From the TEM image, it is shown that the silica spheres were synthesized as size mono-dispersion and the average diameter was approximately 40 nm (Fig. 1A) [28]. Subsequently, the silver shells were deposited on the silica spheres and thickness was estimated to be approximately 10 nm thick from TEM images (Fig. 1B) [29]. The silver nanoshells were protected with organic monolayers of PEG-like ligands and the protected shells therefore were shown to have good chemical stability in PBS buffer [30]. On the other hand, the organic monolayers on the metal nanoshells also prevented them from the nonselective conjugations on the cell surfaces [13,14]. Absorbance spectral measurement of silver nanoshells showed a plasmon resonance at 433 nm (Fig. S2) [19]. The metal nanoshells were partially substituted with (2-mercapto-propionylamino) acetic acid 2,5-dioxo-pyrrolidin-1-ylester *via* ligand exchange reaction, and then covalently bound with Cy5-labelled mAbs via surface reactions [31]. Ensemble emission spectral measurement showed a band centered at 664 nm (Fig. S2) proving that the Cy5-labelled mAbs were indeed bound on the metal nanoshells. A sodium cyanide treatment was used to determine the loading number of mAb on the metal nanoshell [32]. Typically, several drops of NaCN were added into metal nanoshell-containing solution to dissolve the metal. As a result, Cy5-labelled mAb molecules were released from metal nanoshells into solution. According to the molar ratio of metal shell before treatment and free Cy5-labelled mAb after treatment in solution, the loading number could be estimated to be 4.8 on average.

The nanoparticle solution was diluted to nano-mole scale and then cast on the coverslip to prepare the sample for single nanoprobe detection. We believe that most nanoparticles were presented as individuals because of diluted solution. This was furthermore confirmed by the TEM image of nanoparticles (Fig. 1B) on which most nanoparticles were as individuals when the sample was made under the same conditions. The optical properties of these single metal nanoshells were determined on a time-resolved confocal microscope and a representative image was presented in Fig. 1C. As a control, a representative image of metal-free mAb molecule was also shown in Fig. 1D. At least 50 emission signals from the single mAb-Ag complexes as well as metal-free mAb molecules were collected in the emission intensity and lifetime for statistic analysis. The results revealed that on the emission intensity, the mAb-Ag complexes were 15-fold brighter than the Cy5-mAb molecules (Fig. 2A). Considering each metal nanoparticle is bound

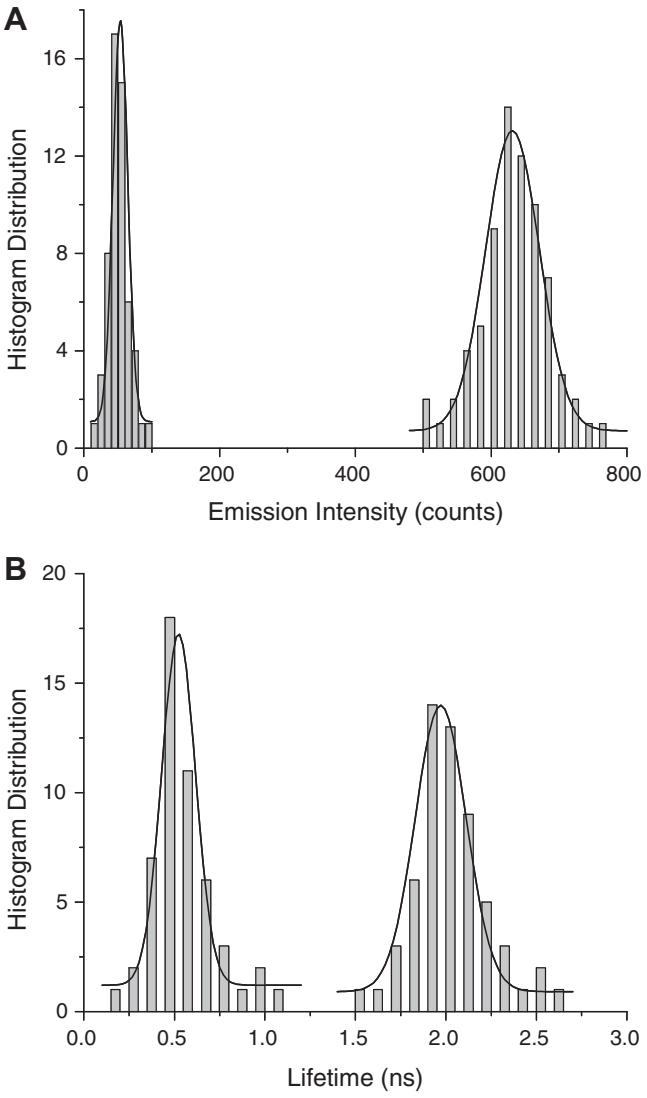

Fig. 2. Histogram distributions of (A) emission intensity and (B) lifetime that were obtained from the emission images by single metal free Cy5-labelled mAbs and mAb-Ag complexes.

by 4.8 mAb molecules, we approximately estimate that the near-field interactions can lead to 3.1-fold enhancement on the emission intensity [11,12]. We also observe that the lifetime of Cy5 on the mAb molecules is dramatically shortened from 2.0 ns to 0.4 ns with binding the mAb molecules on the silver nanoshells (Fig. 2B). It is interesting to notice that the shortened lifetime is significantly less than the value of cellular autofluorescence (2–10 ns), and thus, the emission signals by the metal nanoprobes can be identified from the cellular backgrounds in lifetime cell imaging.

LNCAP and HeLa cells were used to incubate with the mAb-Ag complexes, respectively. The incubation time was 2 h, longer than the time for metal free mAbs (30 min). It is because the nanoparticle probes are bulky in volume and thus need longer time to overcome steric hindrance during immunoreaction with the targets on the cell surfaces [34]. The images of nanoprobe-conjugated cells were recorded in the both emission intensity and lifetime, and representative cell images of LNCAP and HeLa cells were presented in Fig. 3A and B, respectively. With stronger emission intensity and a unique lifetime, it was shown that the emission signals from the mAb-Ag complexes on the cells could be isolated distinctly from the cellular backgrounds on the collected cell images (Fig. 3C).

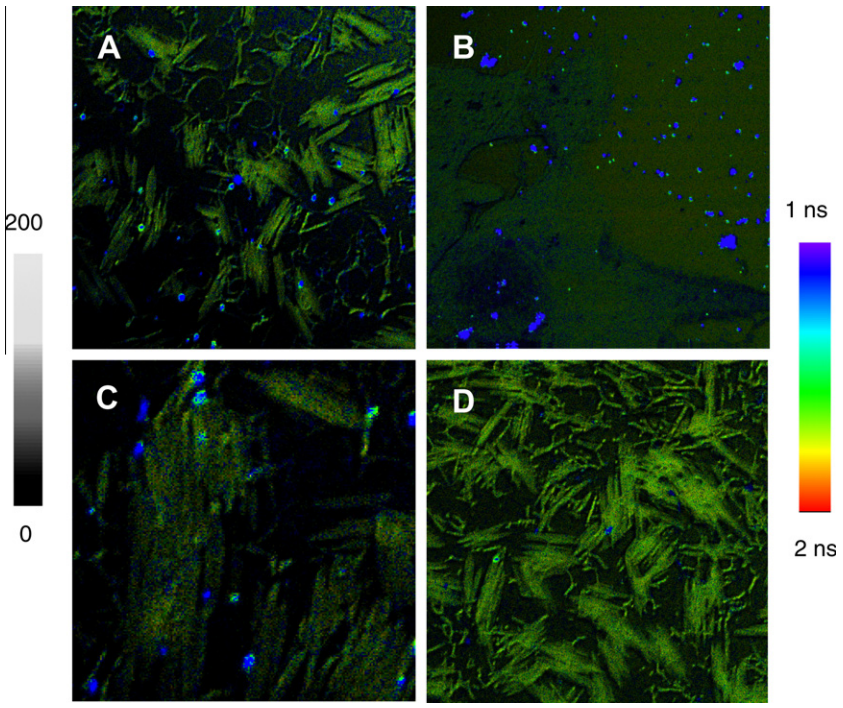

Fig. 3. Representative cell images of (A) LNCAP and (B) HeLa cells that were incubated with the mAb-Ag complexes, as well as (C) single cell image of LNCAP cells that were incubated with the mAb-Ag complexes and (D) representative cell images of LNCAP cells that were incubated with Cy5-IgG mAb-Ag complexes. The scales of (A), (B), and (D) diagrams are 80 × 80 μm and (C) is 20 × 20 μm. The resolutions of diagrams are an integration of 0.6 ms/pixel.

We also noticed that most emission signals from the mAb-Ag complexes were localized within the cellular backgrounds on the images and only few were out, revealing that these mAb-Ag complexes were conjugated in the cells. To confirm the specialty of such conjugations, we also covalently bound Cy5-labelled IgG mAbs on the metal nanoshells in the same strategy and incubated the IgG mAb-Ag complexes with the LNCAP cells. The collected cell images showed significantly less number of emission signals from the metal nanoprobes (Fig. 3D), indicating that the mAb-Ag complexes indeed immunoreacted with the target CK19 molecules on the LNCAP cell surfaces.

It was observed that the emission signals of metal nanoprobes on the single cell images could be counted. To isolate their emission signals precisely, we treated the lifetime cell images with OriginPro7.0 software. Typically, the lifetime dates longer than 1.5 ns were removed from the total lifetime data and the residual data were subsequently recovered back to an image. As a result, most signals from the cellular backgrounds were removed and the emission spots by the metal nanoprobes could be identified more clearly for counting. For each cell sample, at least 20 cell images were treated as described, and the count numbers from the cell images were collected and analyzed with a Gaussian distribution as shown in Fig. 4. The maximal value for LNCAP cells was estimated to be 13. For the control sample of LNCAP cells that were incubated with IgG mAb-Ag complexes, the distribution curve displayed only a direct decay rather than a normal Gaussian distribution and the maximum thus is at zero. This result indicates that the CK19 mAb-Ag complexes display much stronger affinity of immunoreaction with the target CK19 molecules on the cell surfaces.

The HeLa cell images were also treated in the same strategy, and the maximal count number of emission spot on the single cell images was estimated to be 32. From the previous report, it is known that there are approximately 100 CK19 molecules on a single HeLa cell [33]. Therefore, the count number of mAb-Ag complexes on the cell images was significantly fewer than actual expression number of CK19 in the HeLa cells. This is probably

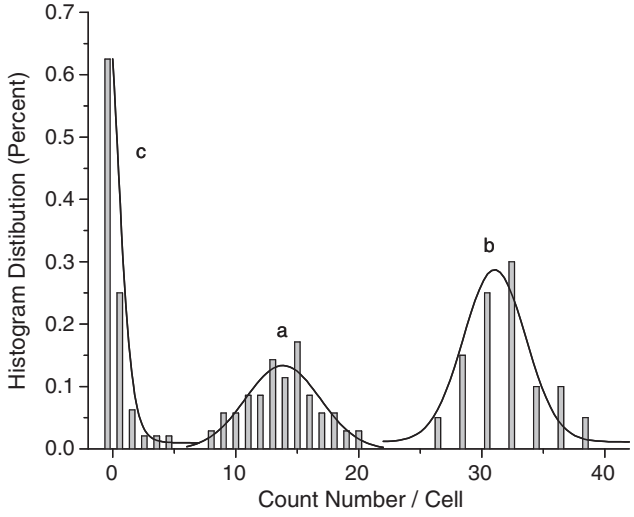

Fig. 4. Histogram distributions of count numbers by the emission spots on the single cell images from (A) LNCAP, (B) HeLa cells, and (C) LNCAP control cell sample incubated with Cy5-IgG mAb-Ag complexes.

due to two reasons. First, the mAb-Ag complexes have multiple mAbs per metal nanoparticle, and thus, may immunoreact with more than one target CK19 molecules in the cells. Second, the *x*–*y* dimensional resolution of confocal microscopy is 200 × 200 nm, which is much larger than the size of mAb-metal complexes. Therefore, one emission spot on the cell image may contain the emission signals from several mAb-metal complexes that cannot be resolved. We cannot examine the exact binding number of CK19 bound with one mAb-Ag complex in this research. Alternatively, we can estimate that one emission signal on the cell image may represent approximately 3.4 molecules of CK19 on the HeLa cell. This estimated number can be used to represent the

immunoreaction capability of metal nanoparticle probes with the target molecules in the cells. For instance, there is yet a report on the expression number of CK19 on LNCAP cell. Currently, we employ the estimated number as reference to calculate the expression number of CK19 on the LNCAP cell that is 44. It indicates that there are approximately 44 of CK19 molecules on a LNCAP cell.

Cytokeratins are expressed in the intermediate filaments in the epithelial cells, so it is reasonable to observe that the CK19 molecules are distributed homogeneously throughout the cell surfaces without significant aggregation on both LNCAP and HeLa cell images.

Nevertheless, a new type of metal nanoshell was synthesized as molecular imaging agent to detect the expression of CK19 molecules in LNCAP and HeLa cells. In this research, the cores of metal shells were reserved as empty. In future, the iron oxide nanoparticles can be encapsulated in the cores to develop multiple-functional nanoparticles for both MRI and fluorescence imaging. We also expect that there are other functional components incorporating in the cores for their more functions. For instance, the metal shells can be used as carriers to load anti-tumour drugs in cores and the delivery of drugs from the cores can be controlled by a light irradiation [34]. The optical properties from the organic dyes on the external layers of metal nanoshells can be used to monitor the in-vivo delivery process in the body.

Acknowledgment

This research was supported by grants from NIH (JZ and RZ: EB009509, JR and JZ: HG-002655, HG005090, CA147975).

Appendix A. Supplementary data

Supplementary data associated with this article can be found, in the online version, at doi:10.1016/j.bbrc.2011.08.042.

References

[1] N.J. Halas, S. Lal, W.-S. Chang, S. Link, P. Nordlander, Plasmons in strongly coupled metallic nanostructures, Chem. Rev. 111 (2011) 3913–3961.
[2] A. Louie, Multimodality imaging Probes: design and challenges, Chem. Rev. 110 (2010) 3146–3195.
[3] M. Mahmoudi, H. Hosseinkhani, M. Hosseinkhani, S. Boutry, A. Simchi, W.S. Journeay, K. Subramani, S. Laurent, Magnetic resonance imaging tracking of stem cells in vivo using iron oxide nanoparticles as a tool for the advancement of clinical regenerative medicine, Chem. Rev. 111 (2011) 253–280.
[4] P. Caravan, Targeted molecular imaging with MRI, medicinal inorganic chemistry, in: ACS Symposium Series, Chapter 11, vol. 903, ACS publications, Washington DC, 2005.
[5] M.A.M. Gijs, F. Lacharme, U. Lehmann, Microfluidic applications of magnetic particles for biological analysis, catalysis, Chem. Rev. 110 (2010) 1518–1563.
[6] S. Laurent, D. Forge, M. Port, A. Roch, C. Robic, L.V. Elst, R.N. Muller, Magnetic iron oxide Nanoparticles: synthesis, Stabilization, vectorization, physicochemical characterizations, and biological applications, Chem. Rev. 108 (2008) 2064–2110.
[7] Z. Xu, Y. Hou, S. Sun, Magnetic core/shell Fe3O4/Au and Fe3O4/Au/Ag nanoparticles with tunable plasmonic properties, J. Am. Chem. Soc. 129 (2007) 8698–8699.
[8] H. Zou, S. Wu, J. Shen, Polymer/silica nanocomposites: preparation, characterization, properties, and applications, Chem. Rev. 108 (2008) 3893–3957.
[9] K. Sokolov, G. Chumanov, T.M. Cotton, Enhancement of molecular fluorescence near the surface of colloidal metal films, Anal. Chem. 70 (1998) 3898–3905.
[10] C. Hubert, A. Rumyantseva, G. Lerondel, J. Grand, S. Kostcheev, L. Billot, A. Vial, R. Bachelot, P. Royer, S.-H. Chang, S.K. Gray, G.P. Wiederrecht, C. Schatz, Near-field photochemical imaging of noble metal nanostructures, Nano Lett. 5 (2005) 615–619.
[11] A.M. Schwartzberg, J.Z. Zhang, Novel optical properties and emerging applications of metal nanostructures, J. Phys. Chem. C 112 (2008) 10323–10337.
[12] R. Stoermer, C.D. Keating, Distance-dependent emission from dye-labeled oligonucleotides on striped Au/Ag nanowires: effect of secondary structure and hybridization efficiency, J. Am. Chem. Soc. 128 (2006) 13243–13254.
[13] S. Lal, S.E. Clare, N.J. Halas, Nanoshell-enabled photothermal cancer therapy: impending clinical impact *Acc*, Chem. Res. 41 (2008) 1842–1851.
[14] K. Jain, X. Huang, I.H. El-Sayed, M.A. El-Sayed, Noble metals on the nanoscale: optical and photothermal properties and applications in imaging, Sensing, biology, and medicine, Acc. Chem. Res. 41 (2008) 1578–1586.
[15] J. Zhang, Y. Fu, G. Li, R.Y. Zhao, J.R. Lakowicz, Direct observation to chemokine receptor 5 on T-lymphocyte cell surface using fluorescent metal nanoprobes, Biochem. Biophys. Res. Comm. 400 (2010) 111–116.
[16] J.R. Lakowicz, Radiative decay engineering: biophysical and biomedical applications, Anal. Biochem. 298 (2001) 1–24.
[17] J.R. Lakowicz, Radiative decay engineering 5: metal-enhanced fluorescence and plasmon emission, Anal. Biochem. 337 (2005) 171–194.
[18] J. Zhang, Y. Fu, M.H. Chowdry, J.R. Lakowicz, Single molecule studies on fluorescently labeled silver particles: effects of particle size, J. Phys. Chem. C 112 (2008) 18–26.
[19] J. Zhang, Y. Fu, J.R. Lakowicz, Luminescent silica core/silver shell encapsulated with Eu(III) complex, J. Phys. Chem. C 113 (2009) 19404–19410.
[20] C.S. Levin, C. Hofmann, T.A. Ali, A.T. Kelly, E. Morosan, P. Nordlander, K.H. Whitmire, N.J. Halas, Magnetic–plasmonic core–shell nanoparticles, ACS Nano 3 (2009) 1379–1388.
[21] J. Ye, N. Verellen, W. Van Roy, L. Lagae, G. Maes, G. Borghs, P. Van Dorpe, Plasmonic modes of metallic semishells in a polymer film, ACS Nano 4 (2010) 1457–1464.
[22] L. Wang, Y. Wang, Y. Liu, M. Cheng, X. Wu, H. Wei, Flow cytometric analysis of CK19 expression in the peripheral blood of breast carcinoma patients: relevance for circulating tumor cell detection, J. Exp. Clin. Cancer Res. 28 (2009) 57.
[23] A. Stathopoulou, I. Vlachonikolis, D. Mavroudis, M. Perraki, C. Kouroussis, S. Apostolaki, N. Malamos, S. Kakolyris, A. Kotsakis, N. Xenidis, D. Reppa, V. Georgoulias, Molecular detection of cytokeratin-19-positive cells in the peripheral blood of patients with operable breast cancer: evaluation of their prognostic significance, J. Clin. Oncol. 20 (2002) 3404–3412.
[24] C. Alix-Panabières, J.P. Vendrell, M. Slijper, O. Pellé1, E. Barbotte, G. Mercier, W. Jacot, M. Fabbro, K. Pantel, Clinical full-length cytokeratin-19 is released by human tumor cells: a potential role in metastatic progression of breast cancer, Breast Cancer Res. 11 (2009) R39.
[25] N. Naseem, N. Reyaz, A.H. Nagi, M. Ashraf, W. Sami, Immunohistochemical expression of cytokeratin-19 in non small cell lung carcinomas – an experience from a tertiary care hospital in Lahore, Int. J. Path. 8 (2010) 54–59.
[26] J. Zhang, D. Roll, C.D. Geddes, J.R. Lakowicz, Aggregation of silver nanoparticle-Dextran adducts with concanavalin A competitive complexation with glucose, J. Phys. Chem. B 104 (2004) 12210–12214.
[27] M.A. Brinkley, Brief survey of methods for preparing protein conjugates with dyes, haptens and crosslinking reagents, Bioconj. Chem. 3 (1992) 2–13.
[28] X. Fang, W. Tan, Aptamers generated from cell-SELEX for molecular medicine: a chemical biology approach, Acc. Chem. Res. 43 (2010) 48–57.
[29] J. Zhang, Y. Fu, J.R. Lakowicz, Emission behavior of Ru(bpy)32+ complex in silver nanoshell – enhanced self-quenching by metal nanostructure, J. Phys. Chem. C 111 (2007) 1955–1961.
[30] A.C. Templeton, W.P. Wuelfing, R.W. Murray, Monolayer-protected cluster molecules, Acc. Chem. Res. 33 (2000) 27–36.
[31] J. Zhang, Y. Fu, D. Liang, K. Nowaczyk, R.Y. Zhao, J.R. Lakowicz, Single cell fluorescence imaging using metal plasmon-coupled probe 2: lifetime image and single molecule counting, Nano Lett. 8 (2008) 1179–1186.
[32] N.L. Rosi, C.A. Mirkin, Nanostructures in biodiagnostics, Chem. Rev. 105 (2005) 1547–1562.
[33] C.H. Chang, L.C. Tsai, S.T. Chen, C.C. Yuan, M.W. Hung, B.T. Hsieh, P.L. Chao, T.H. Tsai, T.W. Lee, Radioimmunotherapy and apoptotic induction on CK19-overexpressing human cervical carcinoma cells with Re-188-mAbCx-99, Anticancer Res. 25 (2005) 2719–2728.
[34] J. Zhang, Y. Fu, J.R. Lakowicz, Metal nanoshell – capsule for light-driven release of small molecule, J. Phys. Chem. C 114 (2010) 7653–7659.